

The dynamics of starvation and recovery

2 Justin D. Yeakel * †‡, Christopher P. Kempes †, and Sidney Redner †§

3 *School of Natural Science, University of California Merced, Merced, CA, †The Santa Fe Institute, Santa Fe, NM, §Department of Physics, Boston University, Boston
4 MA, and ‡To whom correspondence should be addressed: jdyeakel@gmail.com

5 Submitted to Proceedings of the National Academy of Sciences of the United States of America

6 The eco-evolutionary dynamics of species is fundamentally linked
7 to the energetic constraints of its constituent individuals. Of par-
8 ticular importance are the tradeoffs between reproduction and
9 the dynamics of starvation and recovery in resource-limited envi-
10 ronments. To elucidate the consequences of this tradeoff, we
11 introduce a minimal nutritional state-structured model that in-
12 corporates two classes of consumer: nutritionally replete con-
13 sumers that reproduce, and undernourished, non-reproducing
14 consumers that are susceptible to mortality. As a function of the
15 transition rates between these replete and undernourished states
16 that are determined by the presence or absence of resources,
17 the consumer populations can either undergo cyclic dynamics or
18 reach a steady state. We obtain strong constraints on starvation
19 and recovery rates by deriving allometric scaling relationships
20 and find that population dynamics subject to these constraints
21 can approach the cyclic regime but are typically driven to a steady
22 state. Moreover, we find that these rates fall within a ‘refuge’ in pa-
23 rameter space, where the probability of extinction of the consumer
24 population is minimized. Thus we identify a potential mechanism
25 that may both drive and constrain the dynamics of animal pop-
26ulations. Our model provides a natural framework that predicts
27 maximum body size for mammals by determining the relative sta-
28 bility of an otherwise homogeneous population to a mutant pop-
29 ulation with altered percent body fat. For body masses $\lesssim 10^7$ g,
30 a more apidose invader dominates over the resident population,
31 and vice versa for body mass $\gtrsim 10^7$ g, thus providing a principled
32 mechanism for a within-lineage driver of Cope’s rule.

33 foraging | starvation | reproduction

34 Introduction

35 The behavioral ecology of nearly all organisms is influenced by
36 the energetic state of individuals, which directly influences how
37 they invest reserves in uncertain environments. Such behav-
38 iors are generally manifested as tradeoffs between investing in
39 somatic maintenance and growth, or allocating energy towards
40 reproduction [1, 2, 3]. The timing of these behaviors responds
41 to selective pressure, as the choice of the investment impacts
42 future fitness [4]. The influence of resource limitation on an
43 organism’s ability to maintain its nutritional stores may lead to
44 repeated delays or shifts in reproduction over the course of an
45 organism’s life.

46 The balance between (a) somatic growth and maintenance,
47 and (b) reproduction is often conditioned on resource availabil-
48 ity [5]. For example, reindeer invest less in calves born after
49 harsh winters (when the mother’s energetic state is depleted)
50 than in calves born after moderate winters [6]. Many bird
51 species invest differently in broods during periods of resource
52 scarcity compared to normal periods [7, 8], sometimes delaying
53 or even foregoing reproduction for a breeding season [1, 9, 10].
54 Even freshwater and marine zooplankton have been observed to
55 avoid reproduction under nutritional stress [11], and those that
56 do reproduce have lower survival rates [2]. Organisms may also
57 separate maintenance and growth from reproduction over space
58 and time: many salmonids, birds, and some mammals return to
59 migratory breeding grounds to reproduce after one or multiple
60 seasons in resource-rich environments where they accumulate
61 nutritional reserves [12, 13, 14].

62 Physiology also plays an important role in regulating re-
63 productive expenditures during periods of resource limitation.
64 The data collected thus far has shown that diverse mammals (47

65 species in 10 families) exhibit delayed implantation, whereby fe-
66 males postpone fetal development (blastocyst implantation) un-
67 til nutritional reserves can be accumulated [15, 16]. Many other
68 many species (including humans) suffer irregular menstrual cy-
69 cling and higher spontaneous abortion rates during periods of
70 nutritional stress [17, 18]. In the extreme case of unicellular
71 organisms, nutrition is unavoidably linked to reproduction be-
72 cause the nutritional state of the cell regulates all aspects of the
73 cell cycle [19]. The existence of so many independently evolved
74 mechanisms across such a diverse suite of organisms highlights
75 the importance and universality of the fundamental tradeoff
76 between somatic and reproductive investment. However the
77 dynamic implications of these constraints are unknown.

78 Though straightforward conceptually, incorporating the en-
79 ergetic dynamics of individuals [20] into a population-level
80 framework [20, 21] presents numerous mathematical obsta-
81 cles [22]. An alternative approach involves modeling the
82 macroscale relations that guide somatic versus reproductive
83 investment in a consumer-resource system. For example,
84 macroscale Lotka-Volterra models assume that the growth rate
85 of the consumer population depends on resource density, thus
86 implicitly incorporating the requirement of resource availability
87 for reproduction [23].

88 In this work, we adopt an alternative approach in which we
89 explicitly account for resource limitation and the subsequent
90 effect of starvation. Namely, only individuals with sufficient en-
91 ergetic reserves can reproduce. Such a constraint leads to repro-
92 ductive time lags due to some members of the population going
93 hungry and then recovering. Additionally, we incorporate the
94 idea that reproduction is strongly constrained allometrically[3],
95 and is not generally linearly related to resource density. As we
96 shall show, these constraints influence the ensuing population
97 dynamics in dramatic ways.

98 **99 Nutritional state-structured model (NSM)**
100 We begin by defining a minimal Nutritional State-structured
101 population Model (NSM), where the consumer population is
102 partitioned into two states: (a) an energetically replete (full)
103 state F , where the consumer reproduces at a constant rate λ
104 and does not die from starvation, and (b) an energetically de-
105 ficient (hungry) state H , where the consumer does not repro-
106 duce but dies by starvation at rate μ . The underlying resource
107 R evolves by logistic growth with an intrinsic growth rate α
108 and a carrying capacity equal to one. Consumers transition
109 from the full state F to the hungry state H at a rate σ —the

Reserved for Publication Footnotes

starvation rate—and also in proportion to the absence of re-
 sources ($1 - R$). Conversely, consumers recover from state H to state F at rate ρ and in proportion to R . Resources are also eaten by the consumers—at rate ρ by hungry consumers and at rate $\beta < \rho$ by full consumers. This inequality accounts for hungry consumers requiring more resources to replace lost body tissue. The NSM represents a fundamental extension of the idealized starving random walk model of foraging, which focuses on resource depletion, to include reproduction and source replenishment [?, ?, ?].

In the mean-field approximation, in which the consumers and resources are perfectly mixed, their densities evolve according to the rate equations

$$\begin{aligned}\dot{F} &= \lambda F + \rho RH - \sigma(1 - R)F, \\ \dot{H} &= \sigma(1 - R)F - \rho RH - \mu H, \\ \dot{R} &= \alpha R(1 - R) - R(\rho H + \beta F).\end{aligned}$$

Notice that the total consumer density $F + H$ evolves according to $\dot{F} + \dot{H} = \lambda F - \mu H$. This resembles the equation of motion for the predator density in the classic Lotka-Volterra model [?], except that the resource density does not appear in the growth term. As discussed above, the attributes of reproduction and mortality have been explicitly apportioned to the full and hungry consumers, respectively, so that the growth in the total density is decoupled from the resource density.

Equation [1] has three fixed points: two trivial fixed points at $(F^*, H^*, R^*) = (0, 0, 0)$ and $(0, 0, 1)$, and one non-trivial, internal fixed point at

$$\begin{aligned}F^* &= \frac{\alpha\lambda\mu(\mu + \rho)}{(\lambda\rho + \mu\sigma)(\lambda\rho + \mu\beta)}, \\ H^* &= \frac{\alpha\lambda^2(\mu + \rho)}{(\lambda\rho + \mu\sigma)(\lambda\rho + \mu\beta)}, \\ R^* &= \frac{\mu(\sigma - \lambda)}{\lambda\rho + \mu\sigma}.\end{aligned}$$

The stability of this fixed point is determined by the Jacobian matrix \mathbf{J} , where each matrix element $J_{ij} = \partial\dot{X}_i/\partial X_j$ when evaluated at the internal fixed point, and \mathbf{X} is the vector (F, H, R) . The parameters in Eq. [1] are such that the real part of the largest eigenvalue of \mathbf{J} is negative, so that the system is stable with respect to small perturbations from the fixed point. Because this fixed point is unique, it is the global attractor for all population trajectories for any initial condition where the resource and consumer densities are both nonzero.

From Eq. [2], an obvious constraint on the NSM is that the reproduction rate λ must be less than the starvation rate σ , so that R^* is positive. In fact, when the resource density $R = 0$, the rate equation for F gives exponential growth of F for $\lambda > \sigma$. The condition $\sigma = \lambda$ represents a transcritical (TC) bifurcation [?] that demarcates the physical regime from the physical regime where F would grow exponentially with time. The biological implication of the constraint $\lambda < \sigma$ has a simple interpretation—the rate at which a macroscopic organism loses mass due to lack of resources is generally much faster than the rate of reproduction. As we will discuss below, this inequality is a natural consequence of allometric constraints [3] for organisms within empirically observed body size ranges (Fig. 2).

In the physical regime of $\lambda < \sigma$, the fixed point [2] may either be a stable node or a limit cycle (Fig. 3). In continuous-time systems, a limit cycle arises when a pair of complex conjugate eigenvalues crosses the imaginary axis to attain positive real parts [24]. This Hopf bifurcation is defined by $\text{Det}(\mathbf{S}) = 0$, with \mathbf{S} the Sylvester matrix, which is composed of the coefficients of the characteristic polynomial of the Jacobian ma-

stable regime but close to the Hopf bifurcation, the amplitude of the transient but decaying cycles become large. Given that ecological systems are constantly being perturbed [26], the onset of transient cycles, even though they decay with time in the mean-field description, can increase the extinction risk [27, 28, 29]. Thus the distance of a system from the Hopf bifurcation provides a measure of its persistence.

When the starvation rate $\sigma \gg \lambda$, a substantial fraction of the consumers are driven to the hungry non-reproducing state. Because reproduction is inhibited, there is a low steady-state consumer density and a high steady-state resource density. However, if $\sigma/\lambda \rightarrow 1$ from above, the population is overloaded with energetically-replete (reproducing) individuals, thereby promoting oscillations between the consumer and resource densities (Fig. 3).

Whereas the relation between consumer growth rate λ and the starvation rate σ defines an absolute bound of biological feasibility—the TC bifurcation— σ also determines the sensitivity of the consumer population to changes in resource density. When $\sigma \gg \lambda$, the steady-state population density is small, thereby increasing the risk of stochastic extinction. On the other hand, as σ decreases, the system will ultimately be poised either near the TC or the Hopf bifurcation (Fig. 3). If the recovery rate ρ is sufficiently small, the TC bifurcation is reached and the resource eventually is eliminated. If ρ exceeds a threshold value, cyclic dynamics will develop as the Hopf bifurcation is approached.

Role of allometry

While there are no a priori constraints on the parameters in the NSM, most organisms correspond to restricted portions of the parameter space. Here we use allometric scaling relations to constrain the covariation of rates in a principled and biologically meaningful manner. Allometric scaling relations highlight common constraints and average trends across large ranges in body size and species diversity. Many of these relations can be derived from a small set of assumptions and below we describe a

framework to determine the covariation of timescales and rates across the range of mammals for each of the key parameters of our model (cf. [30]). We are thereby able to define the regime of dynamics occupied by the entire class of mammals along with the key differences between the largest and smallest mammals.

Nearly all of the rates described in the NSM are determined by consumer metabolism, which can be used to describe a variety of organismal features [31]. The scaling relation between an organism's metabolic rate B and its body mass M at reproductive maturity is known to scale as $B = B_0 M^\eta$ [32], where the scaling exponent η is typically close to $2/3$ or $3/4$ for metazoans (e.g., [31]), and has taxonomic shifts for unicellular species between $\eta \approx 1$ in eukaryotes and $\eta \approx 1.76$ in bacteria [33, 3]. An organism's metabolic rate B is proportional to the cost of tissue maintenance in the absence of growth (i.e., when the body mass is M). By definition $B = \beta/\xi$, where β is the rate at which resources are consumed for full consumers (see Eq. [1]) and where ξ is related to the conversion efficiency of resource to consumer tissue (Supporting Information, section XX).

Several efforts have shown how a partitioning of B between growth and maintenance purposes can be used to derive a general equation for both the growth trajectories and growth rates of organisms ranging from bacteria to metazoans [34, 35, 36, 37, 3]. This relation is derived from the simple balance condition [34, 35, 36, 37, 3]

$$B_0 m^\eta = E_m \dot{m} + B_m m, \quad [3]$$

222 m is the mass of the organism at any point in its development. 222 of an organism, the above energy balance prescribes the mass
223 This balance has the general solution [38, 3] 223 trajectory of a non-consuming organism:

$$\left(\frac{m(t)}{M}\right)^{1-\eta} = 1 - \left[1 - \left(\frac{m_0}{M}\right)^{1-\eta}\right] e^{-a(1-\eta)t/M^{1-\eta}} \quad [4]$$

$$m(t) = M e^{-a't/M^{1-\eta}}. \quad [9]$$

224 where, for $\eta < 1$, $M = (B_0/B_m)^{1/(1-\eta)}$ is the asymptotic mass,
225 $a = B_0/E_m$, and m_0 is mass at birth. We now use this solution
226 to define the timescale (see [35] for a detailed presentation of
227 these timescales) of reproduction and recovery from starvation.
228 The time that it takes to reach a particular mass ϵM is given
229 by the timescale

$$\tau(\epsilon) = \ln \left[\frac{1 - (m_0/M)^{1-\eta}}{1 - \epsilon^{1-\eta}} \right] \frac{M^{1-\eta}}{a(1-\eta)} \quad [5]$$

230 where we will define values of ϵ to describe a set of rates within
231 our model. For the time to reproduce, $t_\lambda = \tau(\epsilon_\lambda)$, where ϵ_λ is
232 the fraction of the asymptotic mass where an organism is repro-
233 ductively mature and should be close to one (typically $\epsilon_\lambda \approx 0.95$
234 [34]). The growth rate is then given by $\lambda = \ln(v)/t_\lambda$ where v is
235 the number of offspring produced, and for any constant value of
236 ϵ_λ this will scale like $\lambda \propto M^{\eta-1}$ for $M \gg m_0$ [34, 35, 36, 37, 3].

237 The rate of recovery $\rho = 1/t_\rho$ requires that an organism
238 accrues sufficient tissue to transition from the hungry to the
239 full state. Since only certain tissues can be digested for energy
240 (for example the brain cannot be degraded to fuel metabolism),
241 we define the rates for starvation, death, and recovery by the
242 timescales required to reach, or return from, specific fractions of
243 the replete-state mass (see the Supporting Information for de-
244 tails on these parameterizations). We define $m_\sigma = \epsilon_\sigma M$, where
245 $\epsilon_\sigma < 1$ is the fraction of replete-state mass where reproduc-
246 tion ceases. This fraction will be modified if tissue composition
247 systematically scales with adult mass. For example, making
248 use of the observation that body fat in mammals scales with
249 overall body size according to $M_{\text{fat}} = f_0 M^\gamma$ and assuming that
250 once this mass is fully digested the organism starves, this would
251 imply that $\epsilon_\sigma = 1 - f_0 M^\gamma / M$. It follows that the recovery
252 timescale, t_ρ , is the time to go from $m = \epsilon_\sigma \epsilon_\lambda M$ to $m = \epsilon_\sigma M$
253 (Figure 1). Using Eqs. [4] and [5] this timescale is given by
254 simply considering an adjusted starting mass of $m'_0 = \epsilon_\sigma \epsilon_\lambda M$,
255 in which case

$$t_\rho = \ln \left[\frac{1 - (\epsilon_\sigma \epsilon_\lambda)^{1-\eta}}{1 - \epsilon^{1-\eta}} \right] \frac{M^{1-\eta}}{a'(1-\eta)} \quad [6]$$

256 where a' accounts for possible deviations in the biosynthetic en-
257 ergetics during recovery (see Supporting Information). It should
258 be noted that more complicated ontogenetic models explicitly
259 handle storage [37], whereas this feature is implicitly covered
260 by the body fat scaling in our framework.

261 To determine the starvation rate, σ , we are interested in the
262 time required for an organism to go from a mature adult that
263 reproduces at rate λ , to a reduced-mass hungry state where re-
264 production is impossible. For starving individuals we assume
265 that an organism must meet its maintenance requirements using
266 the digestion of existing mass as the sole energy source. This
267 assumption implies the following simple metabolic balance

$$\dot{m}E'_m = -B_m m$$

268 or

$$\dot{m} = -\frac{a'}{M^{1-\eta}} m$$

269 where E'_m is the amount of energy stored in a unit of exist-
270 ing body mass which differs from E_m , the energy required to
271 synthesize a unit of biomass [37]. Given the replete mass, M ,

272 of an organism, the above energy balance prescribes the mass
273 trajectory of a non-consuming organism:

$$t_\sigma = -\frac{M^{1-\eta}}{a'} \ln(\epsilon_\sigma). \quad [10]$$

274 The time scale for starvation is given by the time it takes $m(t)$
275 to reach $\epsilon_\sigma M$, which gives

$$276 \quad \text{The starvation rate is then } \sigma = 1/t_\sigma, \text{ which scales with replete-} \\ 277 \quad \text{state mass as } 1/M^{1-\eta} \ln(1 - f_0 M^\gamma / M). \text{ An important feature} \\ 278 \quad \text{is that } \sigma \text{ does not have a simple scaling dependence on } \lambda, \text{ which} \\ 279 \quad \text{is important for the dynamics that we later discuss.}$$

280 The time to death should follow a similar relation, but de-
281 fined by a lower fraction of replete-state mass, $m_\mu = \epsilon_\mu M$.
282 Suppose, for example, that an organism dies once it has di-
283 gested all fat and muscle tissues, and that muscle tissue scales
284 with body mass according to $M_{\text{musc}} = u_0 M^\zeta$. This gives
285 $\epsilon_\mu = 1 - (f_0 M^\gamma + u_0 M^\zeta) / M$. Muscle mass has been shown
286 to be roughly proportional to body mass [39] in mammals and
287 thus ϵ_μ is merely ϵ_σ minus a constant. The time to death is the
288 total time to reach $\epsilon_\mu M$ minus the time to starve, or

$$t_\mu = -\frac{M^{1-\eta}}{a'} \ln(\epsilon_\mu) - t_\sigma, \quad [11]$$

289 and $\mu = 1/t_\mu$.

290 Although the rate equations [1] are general, here we focus
291 on parameterizations for terrestrial-bound endotherms, specif-
292 ically mammals, which range from a minimum of $M \approx 1$
293 gram (the Etruscan shrew *Suncus etruscus*) to a maximum of
294 $M \approx 10^7$ grams (the late Eocene to early Miocene Indricotheri-
295 inae). Investigating other classes of organisms would simply
296 involve altering the metabolic exponents and scalings associate
297 with ϵ . Moreover, we emphasize that our allometric equations
298 describe mean relationships, and do not account for the (some-
299 times considerable) variance associated with individual species.

300 Stabilizing effects of allometric constraints

301 As the allometric derivations of the NSM rate laws reveal, star-
302 vation and recovery rates are not independent parameters, and
303 the biologically relevant portion of the phase space shown in
304 Fig. 3 is constrained via covarying parameters. Given the pa-
305 rameters of terrestrial endotherms, we find that σ and ρ are
306 constrained to lie within a small window of potential values
307 (Fig. 4) for the known range of body sizes M . We thus find
308 that the dynamics for all mammalian body sizes is confined to
309 the steady-state regime of the NSM and that limit-cycle behav-
310 ior is precluded. Moreover, for larger M , the distance to the
311 Hopf bifurcation increases, while uncertainty in allometric pa-
312 rameters (20% variation around the mean; Fig. 4) results in
313 little qualitative difference in the distance to the Hopf bi-
314 furcation. These results suggest that small mammals are more
315 prone to population oscillations—both stable limit cycles and
316 transient cycles—than mammals with larger body size. Thus
317 common for larger species and more common for smaller species,
318 particularly in environments where resources are limiting.

319 **[I don't see the point of the paragraph below.]** Pre-
320 vious studies have used allometric constraints to explain the
321 periodicity of cyclic populations [40, 41, 42], suggesting a pe-
322 riod $\propto M^{0.25}$. However this relation seems to hold only for
323 some species [43], and potential drivers range from predator
324 and/or prey lifespans to competitive dynamics [44, 45]. Sta-
325 tistically significant support for the existence of population cy-
326 cles among mammals is predominantly based on time series for
327 small mammals [46], where our model would predict more pro-
328 nounced transient dynamics, given how close these points are to

331 the Hopf bifurcation. On the other hand, the longer gestational 396 drivers generate selection towards an optimal upper bound of
332 times and the increased difficulty in measurements, precludes 397 roughly 10^7 grams [51], whose value may arise from higher ex-
333 obtaining similar-quality data for larger organisms. 398 tinction risk for large taxa over evolutionary timescales [52].

334 Extinction risk

335 Within our model, higher rates of starvation result in a larger 399 These trends are thought to be driven by a combination of
336 flux of the population to the hungry state. In this state re- 400 climate change and niche availability [54]; however the under-
337 production is absent, thus increasing the likelihood of extinc- 401 pinning energetic costs and benefits of larger body sizes, and
338 tion. From the perspective of population survival, it is the rate 402 how they influence dynamics over ecological timescales, have
339 of starvation relative to the rate of recovery that determines 403 not been explored. We argue that the NSM provides a suitable
340 the long-term dynamics of the various species (Fig. 3). We 404 framework to explore these issues.
341 therefore examine the competing effects of cyclic dynamics vs.
342 changes in steady state density on extinction risk as a function
343 of the ratio σ/ρ . To this end, we computed the probability of ex-
344 tinction, where we define extinction as a population trajectory
345 falling below one fifth of the allometrically constrained steady
346 state at any time between 10^6 and $\leq 10^8$. This procedure is re-
347 peated for 1000 replicates of the continuous-time system shown
348 in Eq. 1 for an organism of $M = 100$ grams. In each repli-
349 cate the initial densities are chosen to be $A(F^*, H^*, R^*)$, with
350 A a random variable that is uniformly distributed in $[0, 2]$. By
351 allowing the rate of starvation to vary, we assessed extinction
352 risk across a range of values of σ/ρ between ca. 10^{-3} to 5, thus
353 examining a horizontal cross-section of Fig. 3. As expected,
354 higher rates of extinction correlate with both low and high val-
355 ues of σ/ρ . For low values of σ/ρ , the increased extinction
356 risk results from transient cycles with larger amplitudes as the
357 system nears the Hopf bifurcation (Fig. 5). For large values
358 of σ/ρ , higher extinction risk arises because of the decrease in
359 the steady state consumer population density. This interplay
360 creates an ‘extinction refuge’ as shown in Fig. 5, such that for
361 a constrained range of σ/ρ , extinction probabilities are mini-
362 mized.

363 We find that the allometrically constrained values of σ/ρ
364 (with 20% variability around energetic parameter means) fall
365 within the extinction refuge. These values are close enough to
366 the Hopf bifurcation to avoid low steady state densities, and
367 far enough away to avoid large-amplitude transient cycles. The
368 fact that allometric values of σ and ρ fall within this relatively
369 small window supports the possibility that a selective mech-
370 anism has constrained the physiological conditions that drive
371 starvation and recovery rates within populations. Such a mech-
372 anism would select for organism physiology that generates ap-
373 propriate σ and ρ values that avoid extinction. This selection
374 could occur via the tuning of body fat percentages, metabolic
375 rates, and biomass maintenance efficiencies. To summarize,
376 our finding that the allometrically-determined parameters fall
377 within this low extinction probability region suggests that the
378 NSM dynamics may both drive—and constrain—natural ani-
379 mal populations.

380 Dynamic and energetic barriers to body size

381 Metabolite transport constraints are widely thought to place
382 strict boundaries on biological scaling [47, 48, 31] and thereby
383 lead to specific predictions on the minimum possible body size
384 for organisms [49]. Above this bound, a number of energetic and
385 evolutionary mechanisms have been explored to assess the costs
386 and benefits associated with larger body masses, particularly
387 for mammals. One important such example is the *fasting en-*
388 *durance hypothesis*, which contends that larger body size, with
389 consequent lower metabolic rates and increased ability to main-
390 tain more endogenous energetic reserves, may buffer organisms
391 against environmental fluctuations in resource availability [50].
392 Over evolutionary time, terrestrial mammalian lineages show a
393 significant trend towards larger body size (known as Cope’s
394 Rule) [51, 52, 53, 54], and it is thought that within-lineage
395

405 The NSM correctly predicts that species with smaller
406 masses have larger steady-state population densities (Fig. 6a).
407 It should also be noted that R^* is decreasing for increasing body
408 size. From the perspective of classic resource competition the-
409 ory we would expect that the species that can live on the lowest
410 resource abundance should outcompete others [55, 56, 57]. The
411 NSM then predicts that larger mammals should outcompete
412 smaller ones, supporting Cope’s rule. This is a natural conse-
413 quence of the steady-state dynamics combined with the derived
414 timescales.

415 Furthermore, many previous studies have focused on the en-
416 ergy equivalence hypothesis which argues that the total energy
417 use, B_{tot} , of a population is constant independent of species
418 size (e.g. [58, 59]). This hypothesis is based on observations
419 showing that the abundance, N , of a species is proportional
420 to the inverse of individual metabolism (e.g. $N \propto M^{-3/4}/B_0$)
421 (e.g. [58, 59]). This is usually stated as $B_{tot} = NB = \text{constant}$
422 which has been shown to hold in mammalian and vascular plant
423 communities (e.g. [58, 59]). Figure ?? shows that both F^* and
424 H^* scale like $M^{-\eta}$ over a wide range of organism sizes and
425 Figure ?? shows that F^*B is a constant over this same range.
426 This result is remarkable because it illustrates that the steady
427 state values of the NSM combined with the derived timescales
428 naturally give rise to the energy equivalence result. Further-
429 more, the equivalence breaks down at distinct sizes at both the
430 large and small end of mammals suggesting that these are hard
431 limits on mammalian body sizes because organisms outside this
432 range do not meet the constant efficiency obeyed by other pop-
433ulations. Significant deviations from constant energy use occur
434 at $M \lesssim 1$ at the small end of mammals and $M \approx 6.5 * 10^7$
435 for the large end. Compellingly, this dynamic bound, which
436 is determined by the rate of energetic recovery, is close to the
437 minimum observed mammalian body size of ca. 1.3–2.5 grams
438 (Fig. 6b,c), a range that occurs as the recovery rate begins
439 its decline. In addition to known transport limitations [49], we
440 suggest that an additional constraint of lower body size stems
441 from the dynamics of starvation. This result mirrors other ef-
442 forts [3, 60] where at a given scale multiple limitations constrain
443 the smallest possibilities for life within a class of organisms.

444 A additional theoretical upper bound on mammalian body
445 size is given by $\epsilon = 0$, where mammals are entirely composed of
446 metabolic reserves, and this occurs at a size of $M = 8.3 \times 10^8$,
447 or $4.5 \times$ the mass of a blue whale. We determine a more real-
448 istic upper bound to body mass by assessing the susceptibility
449 of an otherwise homogeneous population to invasion by a mu-
450 nicipated subset of the population (denoted by $'$) where individuals
451 have a modified proportion of body fat $M' = M(1 + \chi)$ where
452 $\chi \in [-0.5, 0.5]$, thus altering the rates of starvation σ , recov-
453 ery ρ , and maintenance β . There is no internal fixed point
454 that correspond to a state where both original residents and
455 invaders coexist (except for the trivial state $\chi = 0$). To assess
456 the susceptibility to invasion as a function of the invader mass,
457 we determine which consumer has a higher steady-state den-
458 sity for a given value of χ . We find that for $1 \leq M < 10^6$ g,
459 having additional body fat ($\chi > 0$) results in a higher steady-
460 state invader population density ($H'^* + F'^* > H^* + F^*$). Thus
461 the invader has an intrinsic advantage over the resident popu-

462 lation. However, for $M > 10^6$, leaner individuals ($\chi < 0$) have 485 findings, suggest that the modern diversity of mammals may
463 advantageous steady state densities. 486 not represent a true steady state the current distribution of

464 The observed switch in susceptibility as a function of χ at 487 nutrients and large seeds may be very different from the past
465 $M_{\text{opt}} \approx 10^6$ thus serves as an attractor, or an uninvadible evo- 488 [61, 62, 63].

466 lutionary stable state, such that the NSM predicts organismal 489 The energetics associated with somatic maintenance,
467 mass to increase if $M < M_{\text{opt}}$ and decrease if $M > M_{\text{opt}}$. More- 490 growth, and reproduction are important elements that influence
468 over, M_{opt} , which is entirely determined by the population-level 491 the dynamics of all populations [9]. The NSM is a minimal and
469 consequences of energetic constraints, is within an order of mag- 492 general model that incorporates the dynamics of starvation that
470 nitude of the mass observed in the North American mammalian 493 are expected to occur in resource-limited environments. By in-
471 fossil record [51] and also the mass predicted from an evolution- 494 corporating allometric relations between the rates in the NSM,
472 ary model of body size evolution [52]. While the state of the 495 we found: (i) different organismal masses have distinct popu-
473 environment, as well as the competitive landscape, will deter- 496 lation dynamic regimes, (ii) allometrically-determined rates of
474 mine whether specific body sizes are selected for or against [54], 497 starvation and recovery appear to minimize extinction risk, and
475 we suggest that the starvation dynamics outlined here may pro- 498 (iii) the dynamic consequences of these rates may place addi-
476 vide the driving mechanism for the evolution of larger body size 499 tional barriers on the evolution of minimum and maximum body
477 among terrestrial mammals. 500 size. We suggest that the NSM offers a means by which the dy-

478 One might be concerned a greater number of large mam- 501 namic consequences of energetic constraints can be assessed us-
479 mals are currently not observed in the modern world given that 502 ing macroscale interactions between and among species. Future
480 larger mammals are less susceptible to extinction. However, 503 efforts will involve exploring the consequences of these dynamics
481 recent research suggests that the pleistocene may have been 504 in a spatially explicit framework, thus incorporating elements
482 much more populated with a significant diversity of very large 505 such as movement costs and spatial heterogeneity, which may
483 mammals [61, 62, 63] which were also much more geographi- 506 elucidate additional tradeoffs associated with the dynamics of
484 cally widespread than today. These results, combined with our 507 starvation.

- 508 1. Martin TE (1987) Food as a Limit on Breeding Birds: A Life-History Perspective. *Ecol. Annu. Rev. Ecol. Syst.* 18:453–487.
- 509 2. Kirk KL (1997) Life-History Responses to Variable Environments: Starvation and Reproduction in Planktonic Rotifers. *Ecology* 78:434–441.
- 510 3. Kempes CP, Dutkiewicz S, Follows MJ (2012) Growth, metabolic partitioning, and the size of microorganisms. *PNAS* 109:495–500.
- 511 4. Mangel M, Clark CW (1988) *Dynamic Modeling in Behavioral Ecology* (Princeton University Press, Princeton).
- 512 5. Morris DW (1987) Optimal Allocation of Parental Investment. *Oikos* 49:332.
- 513 6. Tveraa T, Fauchald P, Henaug C, Yoccoz NG (2003) An examination of a compensatory relationship between food limitation and predation in semi-domestic reindeer. *Oecologia* 137:370–376.
- 514 7. Daan S, Dijkstra C, Drent R, Meijer T (1988) *Food supply and the annual timing of avian reproduction*.
- 515 8. Jacot A, Valcu M, van Oers K, Kempenaers B (2009) Experimental nest site limitation affects reproductive strategies and parental investment in a hole-nesting passerine. *Animal Behaviour* 77:1075–1083.
- 516 9. Stearns SC (1989) Trade-Offs in Life-History Evolution. *Funct. Ecol.* 3:259.
- 517 10. Barboza P, Jorde D (2002) Intermittent fasting during winter and spring affects body composition and reproduction of a migratory duck. *J Comp Physiol B* 172:419–434.
- 518 11. Threlkeld ST (1976) Starvation and the size structure of zooplankton communities. *Freshwater Biol.* 6:489–496.
- 519 12. Weber TP, Ens BJ, Houston AI (1998) Optimal avian migration: A dynamic model of fuel stores and site use. *Evolutionary Ecology* 12:377–401.
- 520 13. Mduma SAR, Sinclair ARE, Hilborn R (1999) Food regulates the Serengeti wildebeest: a 40-year record. *J. Anim. Ecol.* 68:1101–1122.
- 521 14. Moore JW, Yeakel JD, Peard D, Lough J, Beere M (2014) Life-history diversity and its importance to population stability and persistence of a migratory fish: steelhead in two large North American watersheds. *J. Anim. Ecol.* 83:1035–1046.
- 522 15. Mead RA (1989) in *Carnivore Behavior, Ecology, and Evolution* (Springer US, Boston, MA), pp 437–464.
- 523 16. Sandell M (1990) The Evolution of Seasonal Delayed Implantation. *The Quarterly Review of Biology* 65:23–42.
- 524 17. Bulik CM, et al. (1999) Fertility and Reproduction in Women With Anorexia Nervosa. *J. Clin. Psychiatry* 60:130–135.
- 525 18. Trites AW, Donnelly CP (2003) The decline of Steller sea lions *Eumetopias jubatus* in Alaska: a review of the nutritional stress hypothesis. *Mammal Review* 33:3–28.
- 526 19. Glazier DS (2009) Metabolic level and size scaling of rates of respiration and growth in unicellular organisms. *Funct. Ecol.* 23:963–968.
- 527 20. Kooijman SALM (2000) *Dynamic Energy and Mass Budgets in Biological Systems* (Cambridge).
- 528 21. Sousa T, Domingos T, Poggiale JC, Kooijman SALM (2010) Dynamic energy budget theory restores coherence in biology. *Philos. T. Roy. Soc. B* 365:3413–3428.
- 529 22. Diekmann O, Metz JAJ (2010) How to lift a model for individual behaviour to the population level? *Philos. T. Roy. Soc. B* 365:3523–3530.
- 530 23. Murdoch WW, Briggs CJ, Nisbet RM (2003) *Consumer-resource Dynamics, Monographs in population biology* (Princeton University Press).
- 531 24. Guckenheimer J, Holmes P (1983) *Nonlinear oscillations, dynamical systems, and bifurcations of vector fields* (Springer, New York).
- 532 25. Gross T, Feudel U (2004) Analytical search for bifurcation surfaces in parameter space. *Physica D* 195:292–302.
- 533 26. Hastings A (2001) Transient dynamics and persistence of ecological systems. *Ecol. Lett.* 4:215–220.
- 534 27. Neubert M, Caswell H (1997) Alternatives to resilience for measuring the responses of ecological systems to perturbations. *Ecology* 78:653–665.
- 535 28. Caswell H, Neubert MG (2005) Reactivity and transient dynamics of discrete-time ecological systems. *Journal of Difference Equations and Applications* 11:295–310.
- 536 29. Neubert M, Caswell H (2009) Detecting reactivity. *Ecology*.
- 537 30. Yodzis P, Innes S (1992) Body Size and Consumer-Resource Dynamics. *Am. Nat.* 139:1151–1175.
- 538 31. Brown J, Gillooly J, Allen A, Savage V, West G (2004) Toward a metabolic theory of ecology. *Ecology* 85:1771–1789.
- 539 32. West GB, Woodruff WH, Brown JH (2002) Allometric scaling of metabolic rate from molecules and mitochondria to cells and mammals. *Proc. Natl. Acad. Sci. USA* 99 Suppl 1:2473–2478.
- 540 33. DeLong JP, Okie JG, Moses ME, Sibly RM, Brown JH (2010) Shifts in metabolic scaling, production, and efficiency across major evolutionary transitions of life. *PNAS* 107:12941–12945.
- 541 34. West GB, Brown JH, Enquist BJ (2001) A general model for ontogenetic growth. *Nature* 413:628–631.
- 542 35. Moses ME, et al. (2008) Revisiting a Model of Ontogenetic Growth: Estimating Model Parameters from Theory and Data. <http://dx.doi.org.proxy.lib.sfu.ca/10.1086/679735> 171:632–645.
- 543 36. Gillooly JF, Charnov EL, West GB, Savage VM, Brown JH (2002) Effects of size and temperature on developmental time. *Nature* 417:70–73.
- 544 37. Hou C, et al. (2008) Energy Uptake and Allocation During Ontogeny. *Science* 322:736–739.
- 545 38. Bettencourt LMA, Lobo J, Helbing D, Kuhnert C, West GB (2007) Growth, innovation, scaling, and the pace of life in cities. *Proc. Natl. Acad. Sci. USA* 104:7301–7306.
- 546 39. Folland JP, Mc Cauley TM, Williams AG (2008) Allometric scaling of strength measurements to body size. *Eur J Appl Physiol* 102:739–745.
- 547 40. Calder III WA (1983) An allometric approach to population cycles of mammals. *J. Theor. Biol.* 100:275–282.
- 548 41. Peterson RO, PAGE RE, DODGE KM (1984) Wolves, Moose, and the Allometry of Population Cycles. *Science* 224:1350–1352.
- 549 42. Kruskopis G, Schaffer WM (1991) Population cycles in mammals and birds: Does periodicity scale with body size? *J. Theor. Biol.* 148:469–493.
- 550 43. Hendriks AJ, Mulder C (2012) Delayed logistic and Rosenzweig(MacArthur models with allometric parameter setting estimate population cycles at lower trophic levels well. *Ecological Complexity* 9:43–54.
- 551 44. Kendall BE, et al. (1999) Why do populations cycle? A synthesis of statistical and mechanistic modeling approaches. *Ecology* 80:1789–1805.
- 552 45. Höglstedt G, Seldal T, Breistol A (2005) Period length in cyclic animal populations. *Ecology* 86:373–378.
- 553 46. Kendall, Prendergast, Bjornstad (1998) The macroecology of population dynamics: taxonomic and biogeographic patterns in population cycles. *Ecol. Lett.* 1:160–164.
- 554 47. Brown J, Marquet P, Taper M (1993) Evolution of body size: consequences of an energetic definition of fitness. *Am. Nat.* 142:573–584.
- 555 48. West GB, Brown JH, Enquist BJ (1997) A General Model for the Origin of Allometric Scaling Laws in Biology. *Science* 276:122–126.
- 556 49. West GB, Woodruff WH, Brown JH (2002) Allometric scaling of metabolic rate from molecules and mitochondria to cells and mammals. *Proc. Natl. Acad. Sci. USA* 99:2473–2478.

- 611 50. Millar J, Hickling G (1990) Fasting Endurance and the Evolution of Mammalian 630 59. Enquist BJ, Brown JH, West GB (1998) Allometric scaling of plant energetics and
612 Body Size. *Funct. Ecol.* 4:5–12. 631 population density : Abstract : Nature. *Nature* 395:163–165.
613 51. Alroy J (1998) Cope's rule and the dynamics of body mass evolution in North 632 60. Kempes CP, Wang L, Amend JP, Doyle J, Hoehler T (2016) Evolutionary tradeoffs
614 American fossil mammals. *Science* 280:731. 633 in cellular composition across diverse bacteria. *ISME J* 10:2145–2157.
615 52. Clauset A, Redner S (2009) Evolutionary Model of Species Body Mass Diversifica- 634 61. Doughty CE, Wolf A, Malhi Y (2013) The legacy of the Pleistocene megafauna
616 tion. *Phys. Rev. Lett.* 102:038103. 635 extinctions on nutrient availability in Amazonia. *Nature Geosci* 6:761–764.
617 53. Smith F, Boyer A, Brown J, Costa D (2010) The Evolution of Maximum Body Size of 636 62. Doughty CE, et al. (2016) Megafauna extinction, tree species range reduction, and
618 Terrestrial Mammals. *Science*. 637 carbon storage in Amazonian forests. *Ecography* 39:194–203.
619 54. Saarinen JJ, et al. (2014) Patterns of maximum body size evolution in Cenozoic 638 63. Doughty CE, Faurby S, Svenning JC (2016) The impact of the megafauna extinctions
620 land mammals: eco-evolutionary processes and abiotic forcing. *Proc Biol Sci* 639 on savanna woody cover in South America. *Ecography* 39:213–222.
621 281:20132049–20132049.
622 55. Tilman D (1981) Tests of Resource Competition Theory Using Four Species of Lake 640 **ACKNOWLEDGMENTS.** We thank Luis Bettancourt, Eric Libby, and Seth New-
623 Michigan Algae. *Ecology* 62:802–815. 641 some for helpful discussions and comments on the manuscript. J.D.Y. was sup-
624 56. Dutkiewicz S, Follows MJ, Bragg JG (2009) Modeling the coupling of ocean ecology 642 ported by startup funds at the University of California, Merced, and an Omidyar
625 and biogeochemistry. *Global Biogeochem. Cycles* 23:n/a–n/a. 643 Postdoctoral Fellowship at the Santa Fe Institute. C.P.K. was supported by an
626 57. Barton AD, Dutkiewicz S, Flierl G, Bragg J, Follows MJ (2010) Patterns of Diversity 644 Omidyar Postdoctoral Fellowship at the Santa Fe Institute. S.R. was supported
627 in Marine Phytoplankton. *Science* 327:1509–1511. 645 by grants DMR-1608211 and 1623243 from the National Science Foundation,
628 58. Allen AP, Brown JH, Gillooly JF (2002) Global Biodiversity, Biochemical Kinetics, 646 and by the John Templeton Foundation, all at the Santa Fe Institute.
629 and the Energetic-Equivalence Rule. *Science* 297:1545–1548.

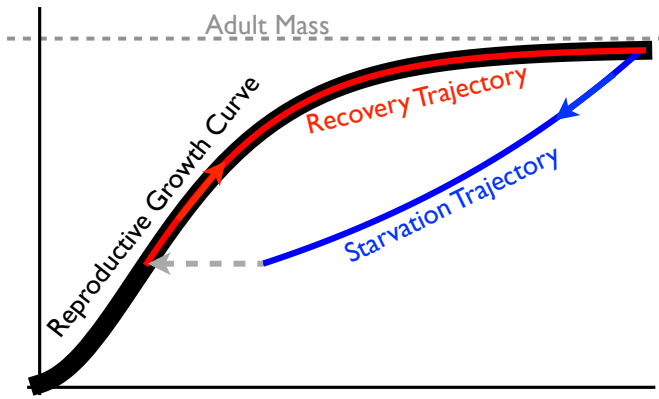


Fig. 1: The growth trajectory over absolute time of an individual organism as a function of body mass. Initial growth follows the red trajectory to an energetically replete adult mass M . Starvation follows the concave blue trajectory to $m_{\text{starve}} < M$, whereas recovery follows the convex growth trajectory from m_σ to M .

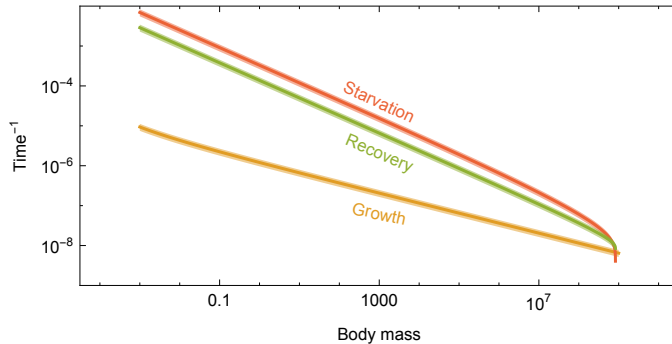


Fig. 2: Allometrically constrained starvation rate σ (red) and recovery rate ρ relative to the reproductive rate λ (yellow) as a function of body mass. The rate of starvation is greater than the rate of reproduction for all realized terrestrial endotherm body sizes. Mean values $\pm 20\%$ variation are shown by the shaded region for each rate.

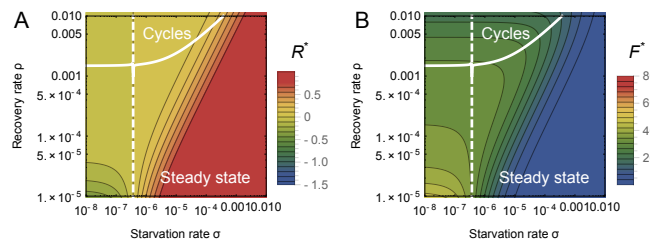


Fig. 3: The transcritical (dashed) and Hopf bifurcation (solid) as a function of the starvation rate σ and recovery rate ρ for a 100 gram consumer. These bifurcation conditions separate parameter space into infeasible, cyclic, and steady state dynamic regimes. The color gradient shows the steady state densities for (A) the resource R^* and the (B) energetically replete consumers F^* , (warmer colors denote higher densities). Steady state densities for the energetically deficient consumers H^* (not shown) scale with those for F^* .

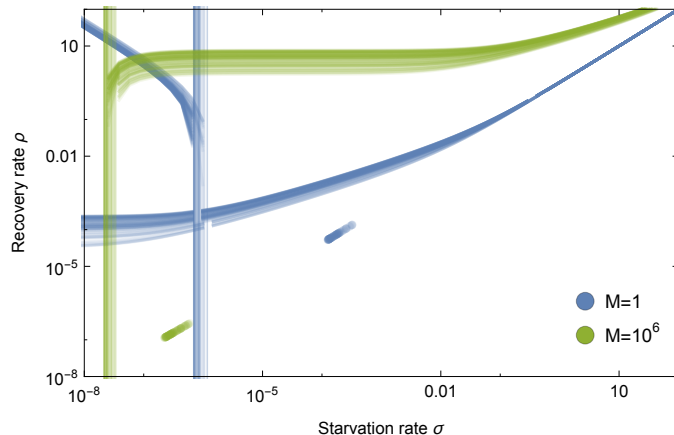


Fig. 4: Transcritical (vertical lines) and Hopf bifurcations (curves) for allometrically determined starvation σ and recovery ρ rates as a function of different mammalian body sizes: $M = A \times 10^1$ gram (blue) and $M = A \times 10^6$ grams (green), where A is a random uniform variable in [1, 9].

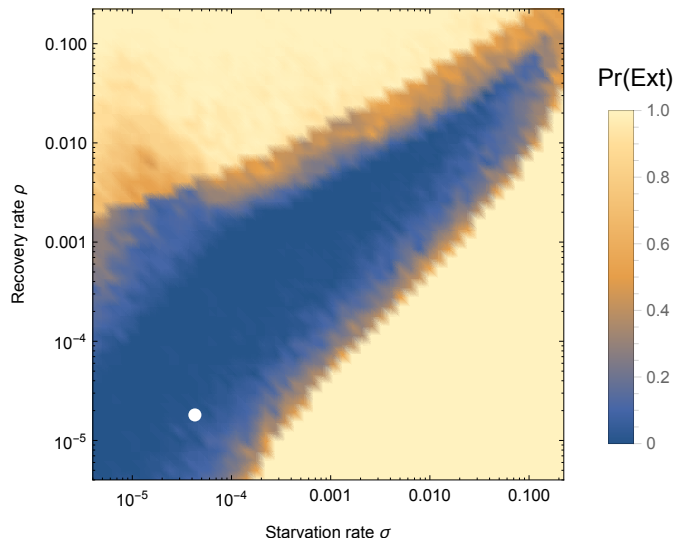


Fig. 5: Probability of extinction for a 100g consumer as a function of the starvation rate σ and recovery rate ρ , where the initial density is given as $A(F^*, H^*, R^*)$, with A being a random uniform variable in [0, 2]. Extinction is defined as the population trajectory falling below $0.1 \times$ the allometrically constrained steady state. The white point denotes the allometrically constrained starvation and recovery rate.

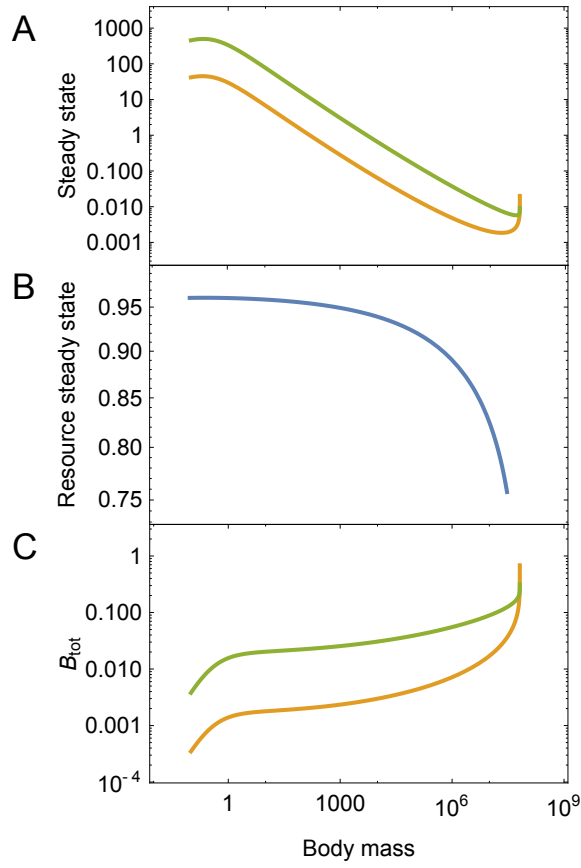


Fig. 6: (A) Consumer steady states F^* and H^* as a function of body mass. (B) Resource steady state R^* as a function of consumer body mass. (C) Total energetic use B_{tot} of consumer populations at the steady state as a function of body mass.

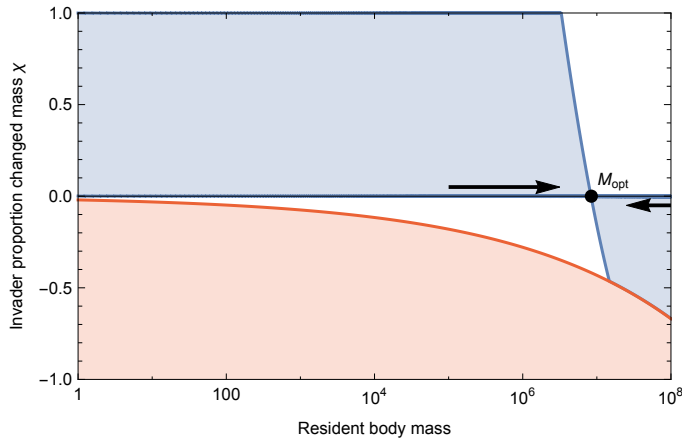


Fig. 7: Invasion feasibility for organisms with a proportional change in mass χ against a population with a resident body mass M . The blue region denotes proportions of modified mass χ resulting in successful invasion. The red region denotes values of χ that result in a mass that is below the starvation threshold and is thus infeasible. Arrows point to the predicted optimal mass $M_{\text{opt}} = 8.43 \times 10^6$, which serves as the evolutionary stable state.